Applied Catalysis B: Environmental 185 (2016) 77–87

Contents lists available at ScienceDirect

Applied Catalysis B: Environmental

journal homepage: www.elsevier.com/locate/apcatb

Alumina supported bimetallic Pt–Fe catalysts applied to glycerol hydrogenolysis and aqueous phase reforming

André Von-Held Soares[a,b], Geronimo Perez[c], Fabio B. Passos[a,*]

[a] Departamento de Engenharia Química e de Petróleo, Universidade Federal Fluminense, Rua Passo da Pátria, 156, Niterói, RJ, CEP 24210-240, Brazil
[b] Instituto Federal do Rio de Janeiro–IFRJ, Avenida República do Paraguai, 120, Sarapuí–Duque de Caxias, RJ, CEP: 25050-100, Brazil
[c] Instituto Nacional de Metrologia (INMETRO), Divisão de Metrologia de Materiais (DIMAT), Av. Nossa Senhora das Graças, no 50, Xerém, Duque de Caxias, RJ, CEP 25250-020, Brazil

ARTICLE INFO

Article history:
Received 10 August 2015
Received in revised form 31 October 2015
Accepted 3 November 2015
Available online 3 December 2015

Keywords:
Glycerol hydrogenolysis
Pt–Fe catalysts
Aqueous phase reforming
Propanediol
Hydrogen

ABSTRACT

Glycerol hydrogenolysis and aqueous phase reforming (APR) are processes that can transform glycerin into 1,2-propanediol (1,2-PD), ethylene glycol (EG), alcohols, ketones and hydrocarbons. This study was performed using five Pt_x–Fe_y/Al_2O_3 catalysts in both glycerol hydrogenolysis and APR reactions, with 2.5%wt. metallic Pt total loading and varying Pt:Fe atomic ratios (1:0; 0:1; 2:1; 1:1; 1:2). The catalysts were analyzed by XRD, TPR, XPS, FT-IR, TEM, N_2 physisorption and H_2 chemisorption, and catalytic tests were undertaken in batch reactions. Except for Fe/Al_2O_3, all catalysts were active for both APR and hydrogenolysis reactions, in which bimetallic Pt_x–Fe_y/Al_2O_3 showed better selectivity towards 1,2-PD than Pt/Al_2O_3. From characterization, it is clear that Pt–Fe interaction displays a pivotal role in enhancing catalytic activity, through the generation of new sites. From the catalytic tests, rate constants and TOF's were calculated. The addition of Fe had a positive effect both in activity and in selectivity for hydrogenolysis towards 1,2-PD. In APR, there is considerable H_2 production, and although activity is greater, there is a slight decline in 1,2-PD production. Through comparison of both reactions' products, it is evident that some of the hydrogen used in glycerol hydrogenolysis comes from glycerol reforming. Glycerol APR over Pt_x–Fe_y/Al_2O_3 catalysts seems to be a viable alternative for low temperature H_2 production.

1. Introduction

The search for fuel alternatives to the fossil derived industry has meant a substantial increase in biodiesel production [1,2] to which new processes have been gradually incorporated as a necessity to deal with the surplus of produced glycerol [3,4]. In the Brazilian context, for instance, a compulsory biodiesel demand has enforced 7% minimum biodiesel content in all diesel fuel consumed in the country, as of November 2014, leading to an increase in the number of authorized production units and actual biodiesel production [5,6]. As of February 2015, the total regulated monthly production of biodiesel in Brazil represented around 47.1% of its total authorized capacity in the country, which represents an increase of 10% compared to February of the previous year. In light of this, glycerol production is still expected to grow.

So far, many processes have been envisaged for glycerol catalytic conversion [4,7], of which dehydration, hydrogenolysis and aqueous phase reforming (APR) reactions are some of the most important. Through these reactions, there is production of many different chemicals including 1,2-propanediol (1,2-PD), 1,3-propanediol (1,3-PD), ethylene glycol (EG), acetone, hydroxyl acetone (acetol), 1-propanol (1-PrOH), 2-propanol (2-PrOH), ethanol and methanol.

Hydrogenolysis can be defined as a reduction reaction involving simultaneous chemical bond dissociation of an organic molecule and hydrogen addition to the generated fragments. Many heterogeneous catalysts and their respective underlying mechanistic rationale have been used in this reaction, yielding different product compositions [7]. For instance, 1,3-PD has been produced over $Ir\text{-}ReO_x/SiO_2$ catalysts with average 67% selectivity, rendering a feasible substitution for its petrochemical production process [8]. By use of bimetallic $Ru–Cu/ZrO_2$ with 1:10 Ru:Cu metallic atomic ratio, 1,2-PD has been produced with 84% selectivity, at the relatively mild temperature of 180 °C [9]. Dehydration processes have produced acrolein over solid heteropolyacids [10], and allyl alcohol over high surface area Fe_2O_3 [11].

Amongst noble metals, platinum catalysts have also been investigated for glycerol hydrogenolysis. Monometallic 5% Pt/C

* Corresponding author. Fax: +55 2126295368.
E-mail address: fbpassos@vm.uff.br (F.B. Passos).

http://dx.doi.org/10.1016/j.apcatb.2015.11.003
0926-3373/

commercial catalyst has shown around 80% selectivity towards 1,2-PD [12,13], at 200 °C, 14–40 bar H_2 initial pressure, outstanding Ru, Pd, Ni, and Cu catalysts, but not copper-cromite catalysts, which exhibited 85% selectivity and 55% glycerol conversion [12]. In one of the first studies performed with Pt catalyzed glycerol hydrogenolysis, Yuan et al. [13] investigated the effect of different supports, reporting unpaired 1,2-PD productivity (92% conversion with 93% selectivity) with Pt/hydrotalcite. They also investigated the Pt (2.0%wt.)/Al_2O_3 catalyst, for which there was a reported conversion of 39% with 81% selectivity towards 1,2-PD at 30 bar H_2 initial pressure, 220 °C and 20 h.

Wawreztz et al. [14] have studied Pt/Al_2O_3 with different Pt loadings in order to investigate the role of particle size in kinetics, proposing that although conversion is slightly affected, product selectivity is strongly influenced by particle size. The authors envisaged three different routes for aqueous phase reforming of glycerol, all of which are initiated with a dehydration step. The increase in particle size disfavored CO_2 and H_2 production, while favoring C2 and C3 oxygenated compounds. Amorphous silica-alumina has also been used as a support for Pt [15] in order to enhance surface area and provide extra acid sites for glycerol dehydration to acetol, and subsequent hydrogen addition at Pt sites, where 1,2-PD and 1-PrOH are produced. Ni/Al_2O_3 produced mainly 1,2-PD, but a small loading of Pt has permitted hydrocracking to EG and methane [16]. Kurosaka et al. [17] reported that the use of Pt/WO_3/ZrO_2 has preferably yielded 1-PrOH and 1,3-PD. They have also proposed that, although working separately, zirconia's acidity and Pt active sites work together for the activation of the glycerol molecule, instead of Pt being exclusively a site for H_2 dissociative chemisorption and subsequent hydrogenation. 1,3-PD has also been produced by the use of sintered Pt–Re/C catalysts [18]. Brandner et al. [19] have used Pt–Sn catalysts for APR, and have noted that platinum based catalysts are of interest because of the hydrogenolysis products generated in this process. Roy et al. [20] have also investigated APR for Pt–Ru/Al_2O_3 catalysts, having found that there is generation of H_2 from heterolytic cleavage of H_2O. The aqueous media has also proved to be fit for 1,3-PD production over Pt/WO_3/TiO_2/SiO_2, with a selectivity of about 50% [21]. Oh et al. [22] researched sulfated zirconia supported platinum catalysts, and have concluded that spillover on Pt sites creates Brønsted acid sites, which drive hydrogenolysis preferably towards 1,3-PD instead of 1,2-PD.

Platinum-based catalysts have also been applied for lactic acid production. Using boric acid as a selectivity promoter, ten Dam et al. [23] found that Pt/$CaCO_3$ yields promising catalytic behavior towards lactic acid, and have also used Pt/Al_2O_3 with tungsten additives to obtain 1,3-PD [24]. Checa et al. [25] studied the use of ZnO and SnO_2 as supports for Au, Pd, Pt, and Rh, noting that the most active catalysts showed strong metal-support interaction (SMSI), yielding lactic acid, instead of 1,2-PD, given metallic alloy formation.

Recent literature points to the use of Pt-based catalysts for APR reactions, among which supported Pt–Ni and Pt–Re catalysts have been investigated for the production of H_2 and other products [26–31]. Within the field of glycerol hydrogenolysis and APR over Pt bimetallic catalysts, specific work on Pt–Fe catalysts is also found [32–34]. Such publications meet the theme of the present work, but only to a certain extent. While Vasiliadou and Lemonidou [32] reported the hydrodeoxygenation of glycerol using ethanol as a hydrogen donor over Pt-catalysts having high iron content; Huber et al. [33] displayed results for ethylene glycol APR over low Fe content Pt-catalysts, mainly interested in H_2 production and gas phase substances; and Lee et al. [34] used Pt–Fe catalysts for aqueous phase hydrogenation (APH) of propanal, xylose, and furfural, saying nothing about glycerol as feed. Therefore, the relationship between H_2 chemisorption, iron content, particle size and activity is not very clear throughout the pertaining references [32–34], leaving aside valuable information for the glycerol hydrogenolysis kinetics. Aiming to fill some of these gaps, this work focuses on Pt_x–Fe_y/Al_2O_3 systems, with low Fe content, their activity in glycerol hydrogenolysis and APR reactions, as well as their characterization.

2. Experimental

2.1. Catalyst preparation

All catalysts were prepared by the incipient wetness impregnation method, using $H_2PtCl_6{\cdot}6H_2O$ and $Fe(NO_3)_3{\cdot}9H_2O$ as precursors for Pt and Fe, respectively, both from Sigma–Aldrich®. Gamma alumina (γ-Al_2O_3) was provided by Sasol® and was calcined at 823 K prior to impregnation. Five catalysts were prepared, two monometallic and three bimetallic catalysts. The ones that contained platinum were prepared using 2.5%wt. Pt loading and varying Fe content to obtain different atom:atom ratios (Pt:Fe), which can be viewed in Table 1. Bimetallic catalysts were co-impregnated, and all catalysts were calcined at 753 K for 4 h at the rate of 5 K/min. Unless stated otherwise, gamma alumina will be referred to throughout this work as Al_2O_3.

2.2. Catalyst characterization

Catalysts were characterized by N_2 physisorption, temperature-programmed reduction (TPR), H_2 chemisorption, X-ray diffraction (XRD), diffusive reflectance infrared Fourier transform spectroscopy (DRIFTS), X-ray photoelectron spectroscopy (XPS), energy dispersive X-ray microanalysis (EDX), and transmission electron microscopy (TEM).

Surface areas and pore volumes were determined by N_2 physisorption at 77 K, using the BET analysis and BJH methods, respectively, employing an ASAP 2020 Micromeritics analyzer. Prior to the measurements, the samples were degassed at 523 K for 6 h.

XRD patterns were performed in a Rigaku (Miniflex II) diffractometer with a CuKα (1.540 Å) radiation.

The temperature programmed reduction (TPR) experiments were performed with samples (0.5 g) that were dried under flow of He (30 mL min^{-1}) for 30 min at 423 K and then cooled to room temperature. Temperature programmed reduction was performed under 30 mL min^{-1} of flowing 5% H_2/Ar while the samples were heated to 723 K at 10 K min^{-1}. The measurements were carried out in a multipurpose unit coupled to a quadrupole mass spectrometer (Pfeiffer Vacuum, Prisma).

Hydrogen chemisorption was performed in a Micromeritics ASAP 2010C automated adsorption analyzer. The samples were reduced at 573 K under flowing H_2 for 60 min, and then outgassed under vacuum at 573 K for an equal period. The catalysts were then cooled to 308 K and the total adsorption isotherm was measured. After the initial adsorption isotherm, the samples were evacuated for 60 min at 308 K and a second isotherm was obtained to determine reversible adsorption. The amount of adsorbed H_2 was calculated by extrapolating the hydrogen uptake to zero pressure, assuming a stoichiometry H/Pt_{surf} equal to unity.

Fourier Transform Infrared (FT-IR) spectroscopy of adsorbed carbon monoxide was performed in a Bruker VERTEX 70 spectrometer with a high-temperature DRIFTS cell (Harrick, HVC-DRP-4), fitted with ZnSe windows, and a diffuse reflectance accessory having a Praying Mantis geometry. Spectra were acquired at a resolution of 4 cm^{-1}, typically averaging 256 scans, which provided the best signal/noise ratio. The samples were initially pretreated with He flow (30 mL min^{-1}) for 30 min at 423 K. Then, the temperature was raised to 573 K in pure H_2 flow (30 mL .min^{-1}) for 1 h. After the reduction, the sample was flushed in He flow for 30 min, fol-

Table 1
Catalysts used in this work.

Catalyst Abbreviation	Description	Pt:Featom:atom ratio	Pt nominal content (%wt.)	Fe nominal content (%wt.)
A	Pt/Al_2O_3	1:0	2.5	0
B	Fe/Al_2O_3	0:1	0	2.5
C	Pt_2–Fe/Al_2O_3	2:1	2.5	0.36
D	Pt–Fe/Al_2O_3	1:1	2.5	0.72
E	Pt–Fe_2/Al_2O_3	1:2	2.5	1.43

lowed by cooling at 303 K. CO adsorption was then performed under CO/He flow (30 mL min^{-1}) for 30 min at 303 K, followed by flushing of the sample for 15 min with He before recording the spectrum. Spectra were recorded at 303 K, 373 K, 473 K, and 573 K.

X-ray photoelectron spectra were taken through scans from selected points of the samples, using ESCALAB 250Xi equipment, and processed by Avantage Data System software, both from Thermo Fischer Scientific. A XR6 monochromatic X-ray gun using 900 μm spot size was employed, under ultra high vacuum ($\sim 10^{-9}$ mbar), with a flood gun for charge neutralization. Powder samples were mounted on top of a holder block using carbon tape. The bonding energy ranges, the number of scans, and the pass energy were selected according to the analyzed element. Dwell time was 50 ms and the energy step size was 0.05 eV. For Pt, since Al2*p* and Pt4*f* lines overlap at the range 65–85 eV, binding energies were also analyzed in the range of 305–345 eV.

EDX analysis was performed using a Shimadzu EDX 720/800HS spectrometer, and TEM experiments were undertaken using a FEI Tecnai G2 Spirit Twin with LaB_6 filament operating at 120 kV.

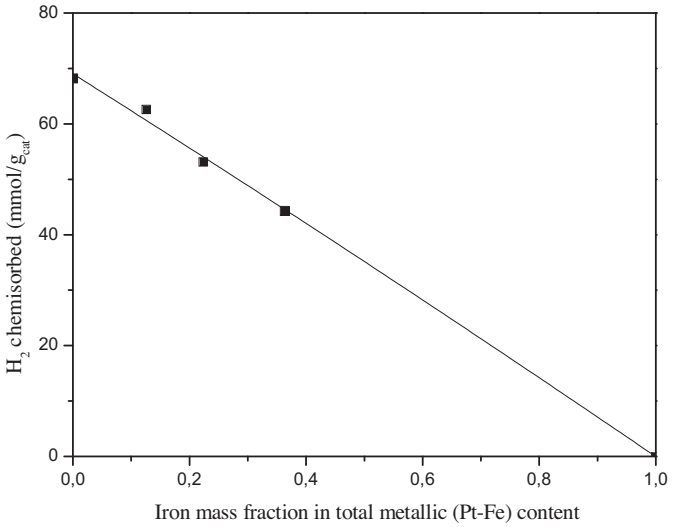

Fig. 1. Irreversible H_2 adsorption uptake as a function of iron mass fraction, $m_{Fe}/(m_{Fe} + m_{Pt})$, Pt_x–Fe_y catalysts.

2.3. Catalytic tests

Glycerol hydrogenolysis reactions were carried out in a benchtop 300 mL stainless steel batch reactor (Parr 4848). For each catalyst, at least three reaction temperatures were tested, namely 473 K, 493 K and 513 K, all of them under initial hydrogen pressure of 26.2 bar, 0.5 g of catalyst and 150 mL of aqueous glycerol solution (20%wt.). The reaction time was 12 h with constant stirring of 500 rpm. At these conditions, the absence of internal mass transfer resistance was confirmed with the Weisz–Prater criterion and external mass transfer limitations were avoided as demonstrated in preliminary experiments by variation of stirring rates.

Prior to the reaction, the catalyst was dried at 423 K and reduced at 723 K for 1 h, in a separate unit, under a flow of pure H_2 (30 mL min^{-1}), followed by passivation at environment atmosphere and temperatures below 273 K, by use of a mixture of ice and liquid N_2 as cooling bath.

The reaction sequence was as follows: loading of the reactor with the glycerol solution and the appropriate amount of catalyst, which was purged under a flow of N_2 (30 mL min^{-1}) for 5 min, and subsequent activation at room temperature under a flow of H_2 (30 mL min^{-1}) for 1 h in the reaction vessel. The temperature and pressure were then increased to the desired values, under constant stirring. The batch reaction proceeded for a 12-h period. After this, the system was cooled to room temperature, and liquid and gaseous samples were collected. Sample collection for kinetics occurred at 30 min intervals after stabilization at the desired temperature, for the first two hours of the reaction.

The liquid phase products were analyzed and identified by a GC–MS (Shimadzu, GCMS-QP2010S) equipped with a 95% polyethyleneglycol (PEG) wax RTX column. The gas phase was sampled and analyzed in a 490 Micro-GC (Agilent) equipped with three columns: M5A 9 (H_2, O_2, N_2, $CH_4$and CO), 5CB (PoraPLOT U CO_2 and C_2H_6) and PPU(CP-Sil 5CB—Hydrocarbons).

Recycling reactions were done for monometallic Pt and bimetallic catalysts, after washing with deionized water, centrifuging for three times, and drying at 493 K for 12–16 h. No further reduction was conducted, and the reaction procedure and conditions were similar to the previously described at a temperature of 493 K for each recycle run.

Glycerol Aqueous Phase Reforming (APR) tests were done for bimetallic catalysts using no external H_2, but only N_2 as an inert gas at an initial pressure of 11.4 bar. The reaction procedure and conditions were similar to the previously described at a temperature of 513 K for each APR run.

3. Results and discussion

3.1. Catalyst characterization

Surface areas, pore dimensions and H_2 chemisorption analysis values are shown in Table 2. In Fig. 1, as well as in Fig. 10, the abscissa shows the values for iron mass fraction in the catalyst metallic phase, namely, $m_{Fe}/(m_{Fe} + m_{Pt})$.

As it can be seen, Fe addition lowers the catalyst's ability to chemically adsorb hydrogen, which is in accordance with the literature [35,36]. For iron content greater than 0.41% (atom) in supported catalysts, it has been reported by Guczi et al. [37] that various iron species are present, being Fe^{3+} and Fe^{2+} on the surface not active towards chemisorptions at environment temperature. All materials' isotherms in this work resemble type II isotherms with H1 hysteresis [38], which are characteristic of unrestricted monolayer–multilayer adsorption, with monolayer coverage occurring very soon in response to the pressure increase, given the smooth transition from the beginning early pressure increases towards quasi-linear adsorption.

XRD analysis was done for all catalysts and for Al_2O_3. The diffractograms of the catalysts are identical to the diffractograms of γ-Al_2O_3 support, from which a very good metallic dispersion may

Table 2
BET areas, BJH pore sizes, H_2 chemisorptions.

Material	BET area (m^2/g)	BJH pore volume (cm^3/g)	Irreversible H_2 uptake (μmol/g)	Reversible H_2 uptake (μmol/g)	Metal dispersion (%)
Al_2O_3	146	0.85	–		–
Pt/Al_2O_3	135	0.80	43.2	24.9	67.4
Fe/Al_2O_3	137	0.73	~0	24.9	–
$Pt_2–Fe/Al_2O_3$	141	0.81	39.6	23.0	61.8
$Pt–Fe/Al_2O_3$	140	0.80	34.0	20.1	53.1
$Pt–Fe_2/Al_2O_3$	138	0.77	28.4	17.5	44.3

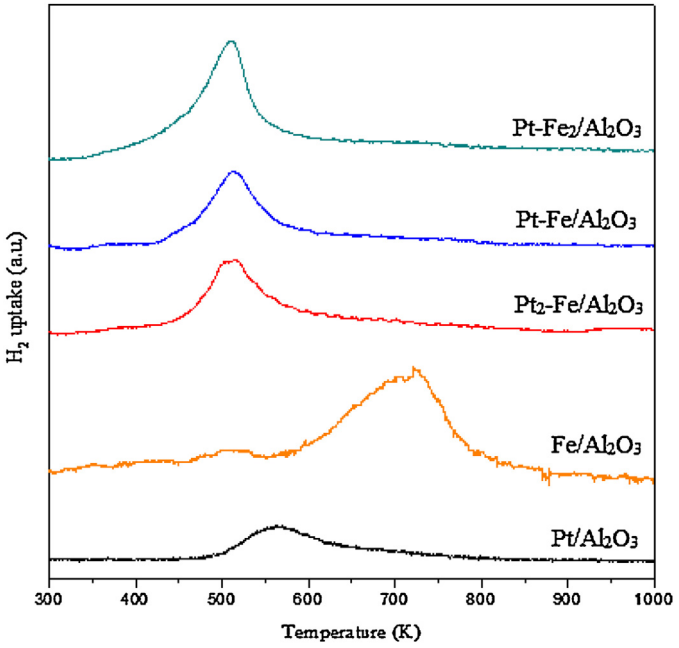

Fig. 2. TPR profiles for Pt/Al_2O_3, Fe/Al_2O_3 and $Pt_x–Fe_y/Al_2O_3$ catalysts.

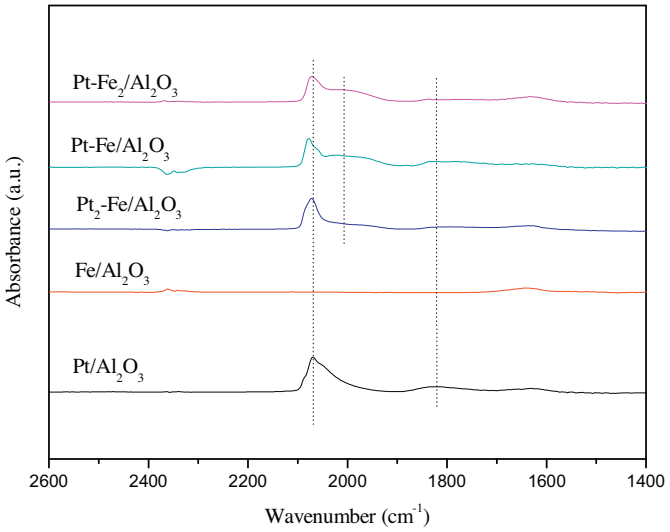

Fig. 3. FT-IR spectra for each of the five $Pt_x–Fe_y/Al_2O_3$ catalysts regarding CO adsorption at 303 K.

be inferred, as the characteristic lines of platinum or iron were not observed.

Temperature programmed reduction (TPR) analyses are shown in Fig. 2. As it can be seen, in the bimetallic $Pt_x–Fe_y$ catalysts there is an increase in the amount of Fe that can be reduced at lower temperatures than with pure Fe. The monometallic Pt catalyst exhibits a broad peak at 560 K, usually ascribed to an oxychloroplatinum complex. For the bimetallic catalysts, hydrogen uptake peaks relatively at the same temperature, around 512 K. The profile for Fe/Al_2O_3 displayed a small peak around 510K and a larger peak centered at 700 K. Fe containing catalysts presented reduction degrees above 100%, for calculations considering PtO_2 and Fe_2O_3, the most oxidized states of both metals. This is evidence for iron aluminate occurrence [39].

Fig. 3 shows DRIFT spectra of adsorbed CO at 303 K for all catalysts. As it can be seen, iron addition to platinum creates new sorts of CO adsorption behavior. The spectra for CO adsorbed on Pt/Al_2O_3 displayed a band at 2061 cm^{-1}, and another broad band at 1820 cm^{-1}, attributed to linear and bridge adsorption modes, respectively [40]. Bimetallic Pt–Fe catalysts exhibited the linear adsorption mode with a shift within the range of 2074–2067 cm^{-1}, and the addition of Fe lead to the presence of a broad shoulder from around 2030 cm^{-1} to 1900 cm^{-1}. This shoulder is most relevant as the iron content is increased, and is clearly indicative of metallic Pt–Fe interaction at the adsorption sites [35,41].

Fig. 4 shows in greater detail the spectra of adsorbed CO obtained for $Pt–Fe/Al_2O_3$ at 303 K, 373 K, 473 K, and 573 K. As it can clearly be seen, the broad band for CO bridge adsorption is substantially weakened by increasing the temperature, while the shoulder created by Fe addition for linear adsorption remains. A band at 2040 cm^{-1} has been attributed reduced Fe linear adsorption [35,39]. As seen in Fig. 4, around this frequency there is a distinct band that overlaps and is more intense than the monometallic Pt tailing peak. As the temperature is increased, the rate of CO desorption increases, as indicated by lower absorbance. However, the Fe reduced sites remain considerably active for CO adsorption in a relative broader band than for the tailing of monometallic Pt sites, throughout the temperature range used for glycerol hydrogenolysis (473–523 K).

The characteristic peaks for XP spectra in the range of 84–65 eV are shown in Fig. 5. Due to overlap of the Al2*p* with the Pt4*f* lines, Al_2O_3-supported Pt catalysts should be analyzed in the range from 305 to 345 eV, where we find the $Pt4d_{5/2}$ and $Pt4d_{3/2}$ lines [42]. Nonetheless, Pt content under 3% displays very poorly resolved peaks. The peaks in Fig. 8 were constructed using a 3.2 eV spacing between $Pt4f_{5/2}$ and $Pt4f_{7/2}$, and a 3:4 intensity ratio [43,44]. By observing Fig. 5, Fe addition seems to move the Pt4f peaks towards lower binding energies, resembling Pt^{2+}. Fig. 6 shows the binding energy range between 345 eV and 305 eV, characteristic of $Pt4d_{5/2}$ and $Pt4d_{3/2}$ lines, for both monometallic Pt/Al_2O_3 and bimetallic $Pt_2–Fe_1/Al_2O_3$ catalysts in the calcined and passivated states. As pointed by the included marking lines, after reduction, the $Pt4d_{5/2}$ peak was clearly shifted towards values characteristic of reduced platinum, lying between the Pt^+ (315 eV) and Pt^0 (314 eV) values [43]. The peak area slightly decreases from calcined to passivated $Pt_2–Fe_1/Al_2O_3$ catalyst, which could be an indication of platinum dilution due to the higher concentration of Fe atoms at the surface. This effect, however, is very mild within the Fe/Pt mass fraction range used in this work.

Fig. 7 shows the EDX spectra for all materials after calcination. As it can be seen, characteristic Fe peaks occurred at 6.39 keV and 7.07 keV, while for Pt they occurred at 9.41, 11.11, and 12.98 keV. The linear relation obtained for the peak heights and metal nomi-

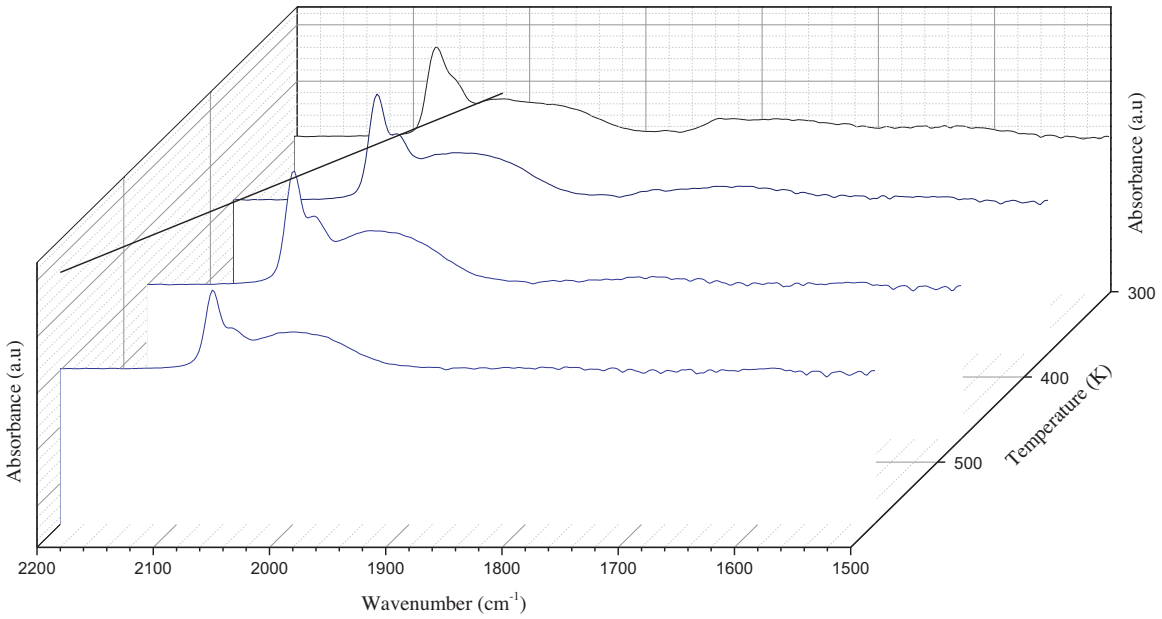

Fig. 4. FT-IR spectra for Pt–Fe/Al_2O_3 regarding CO adsorption at 303 K, 373 K, 473 K, and 573 K.

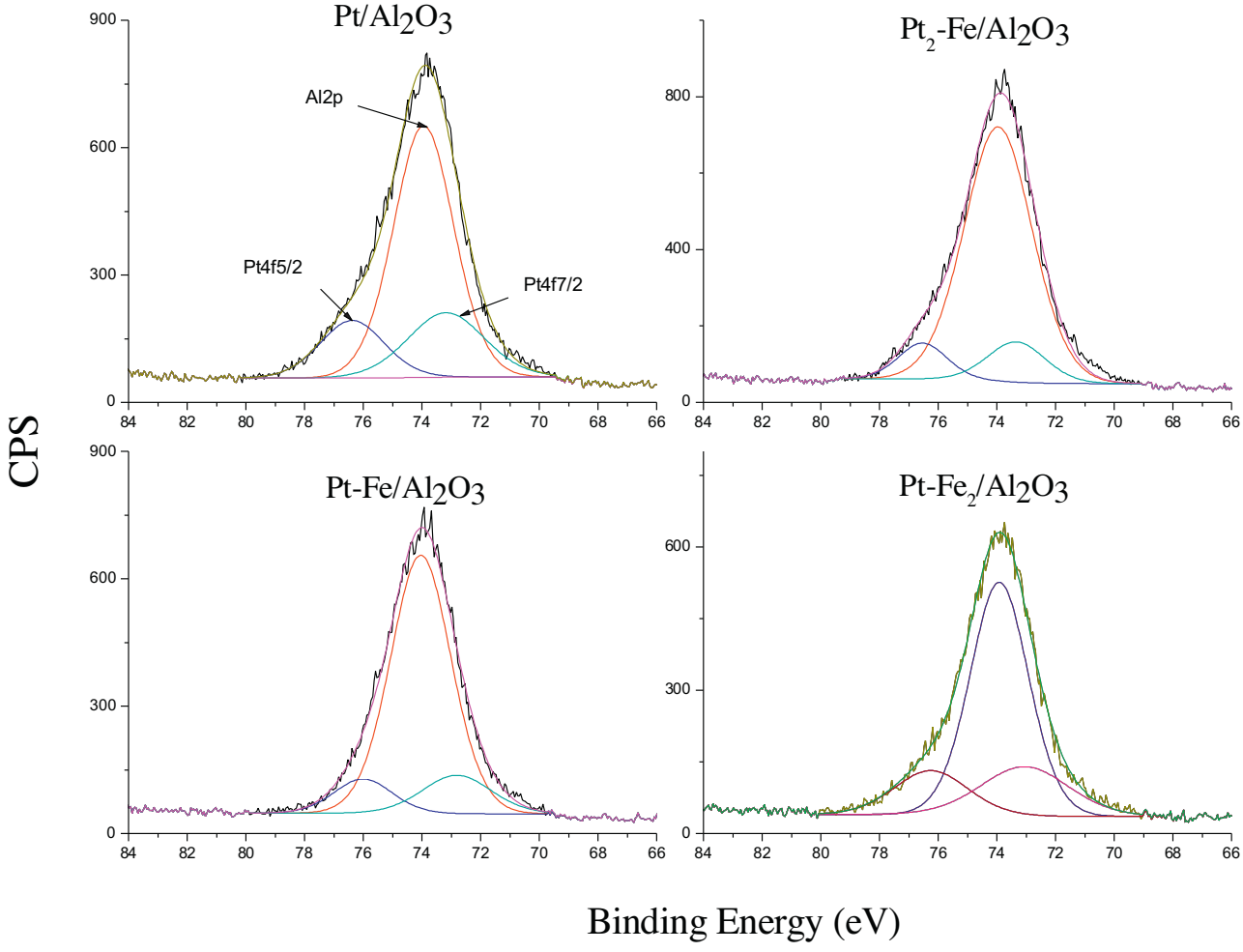

Fig. 5. Al2p scan displaying Pt4$f_{5/2}$ and Pt4$f_{7/2}$ lines for calcined monometallic Pt/Al_2O_3, and bimetallic Pt_x–Fe_y/Al_2O_3 catalysts.

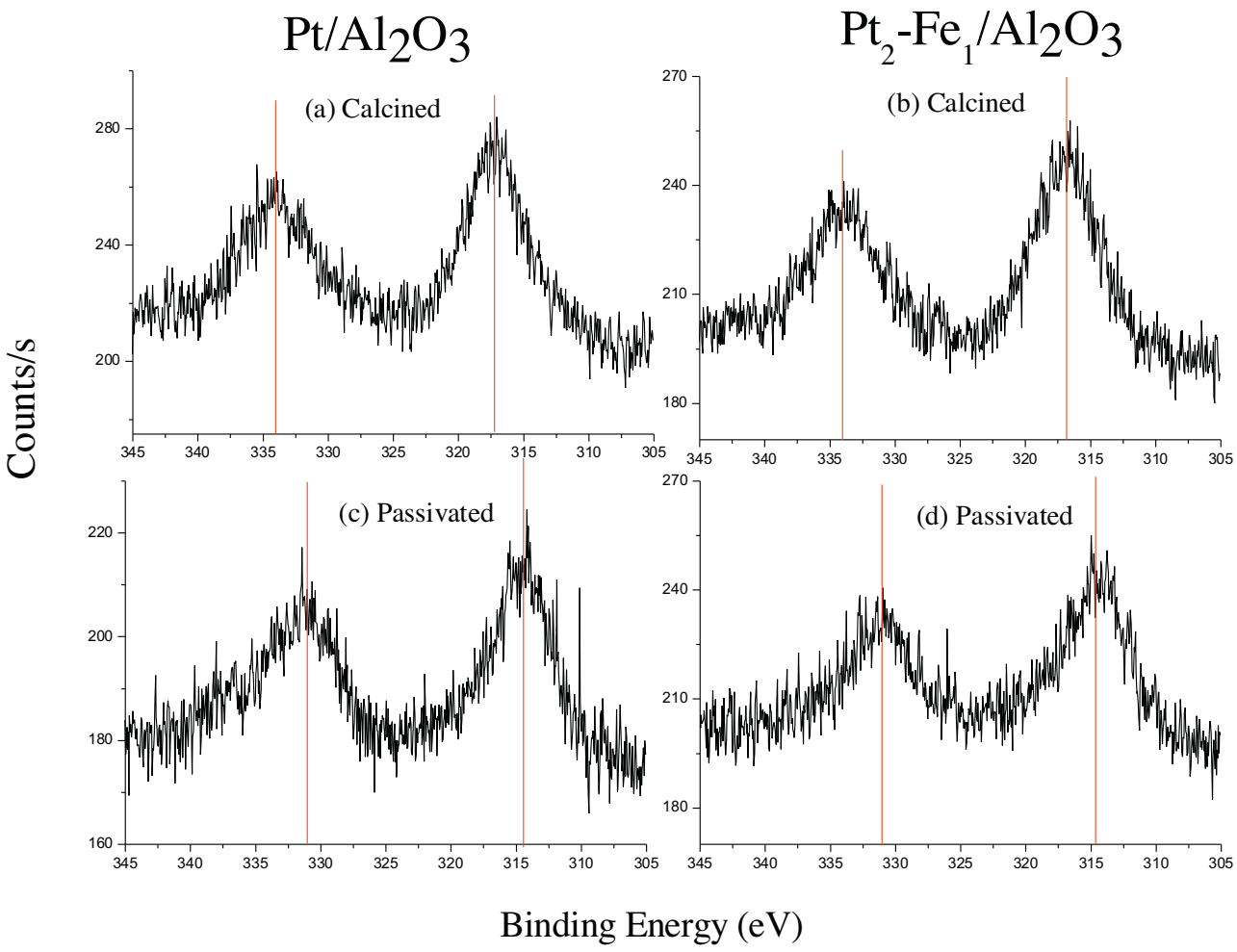

Fig. 6. XP spectra in the range of Pt4*d* peaks for calcined (a and b) and passivated (c and d) catalysts Pt/Al_2O_3 and Pt_2–Fe/Al_2O_3.

nal contents indicates that there was virtually no metal loss in the impregnation process.

Fig. 8 shows TEM micrographs of monometallic and bimetallic catalysts. At the TEM micrograph corresponding to Pt/Al_2O_3 sample (Fig. 8a), it is possible to clearly observe Pt nanoparticles smaller than 10 nm, in dark contrast. For the other samples (Fig. 8b–e) a good contrast between the metal phase and the Al_2O_3 phase was not obtained in order to point the exact metallic catalytic particles' dimensions. This is however in agreement with the XRD analyses, since the impregnated metallic content in all materials was unable to modify the Al_2O_3 pattern. It is also an evidence for very small, well dispersed particles. In the TEM micrograph of Fig. 9, corresponding to Pt/Al_2O_3 sample, the size of the Pt nanoparticles were measured with image processing software and obtained estimated diameter values between 1 and 6 nm approximately. From the data available from Kip et al. [45], the values of particle size from H_2 chemisorption in this work should lie in the range of 1.6–2.5 nm, for the Pt/Al_2O_3 catalyst and for the Pt–Fe_2/Al_2O_3 catalyst, respectively. This is consistent with the TEM particle size estimates. As seen in Table 2, it is worth mentioning that as the H/Pt ratios of H_2 chemisorption decrease with increasing Fe content, the coordination of surface Pt atoms is expected to go higher. It is therefore beyond doubt that there is an increase in particle size in the formation of the bimetallic particles by Fe increment. This affects Pt coordination and thus H/Pt chemisorption ratios, having a direct effect on catalyst activity and selectivity in the glycerol hydrogenolysis reaction.

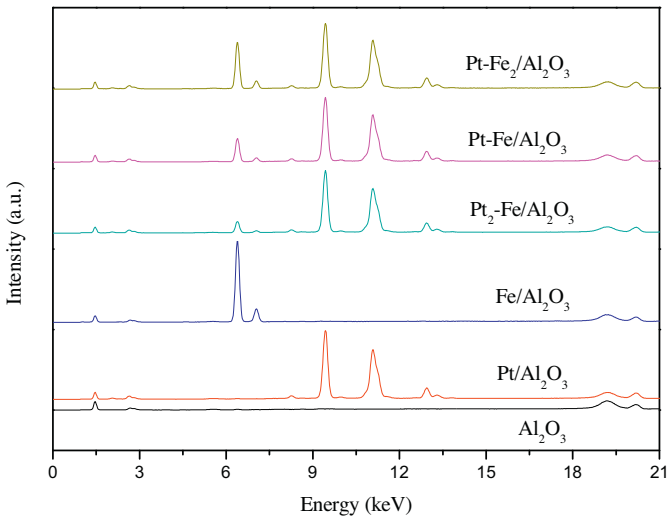

Fig. 7. EDX spectra for Al_2O_3, Pt/Al_2O_3, Fe/Al_2O_3 and Pt_x–Fe_y/Al_2O_3 catalysts.

3.2. Catalytic tests

For the calculation of the Weisz–Prater criterion [46], conservative parameter values were used. Since the catalyst was used as a powder, the characteristic length was considered to be 50 μm, and the density used was 3.95 g/cm^3, both from com-

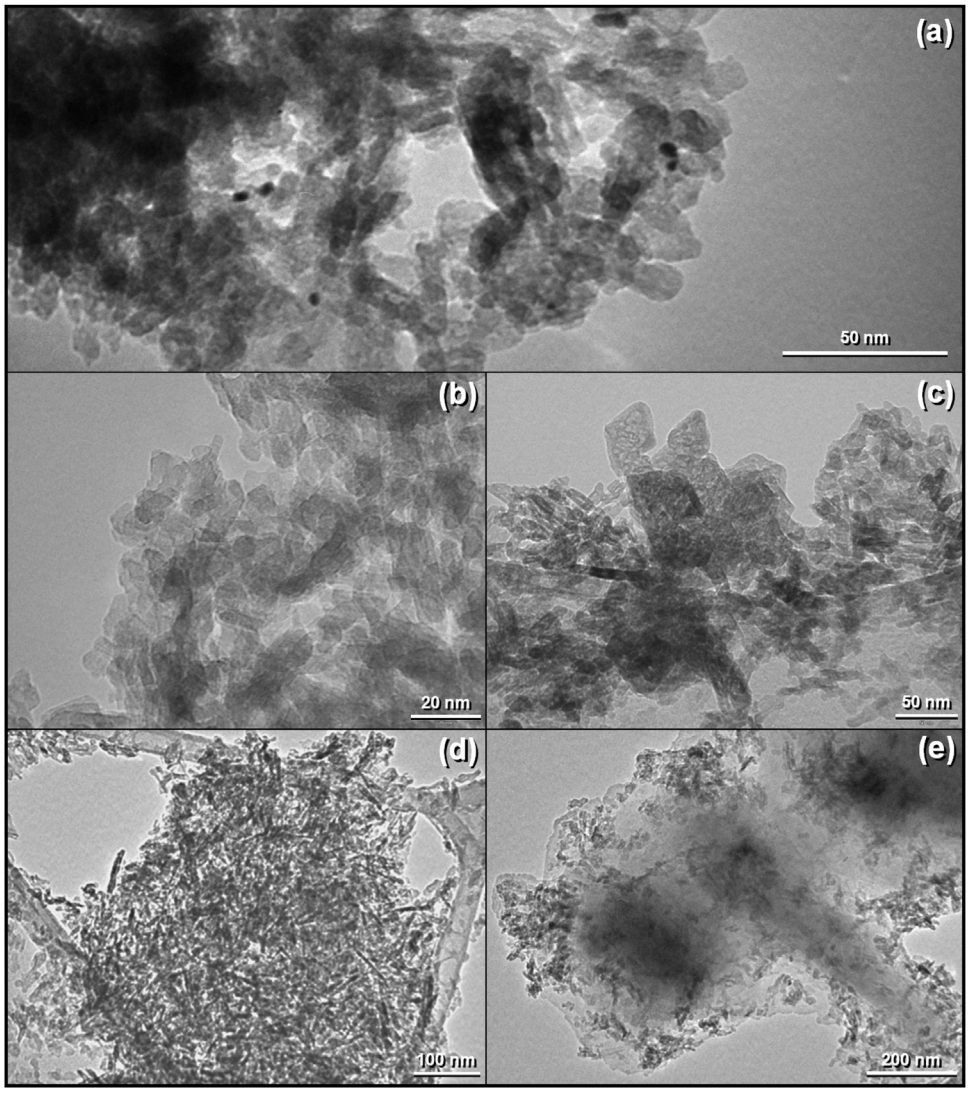

Fig. 8. TEM micrographs of monometallic and bimetallic Pt_x–Fe_y/Al_2O_3 catalysts: (a) Pt/Al_2O_3, (b) Fe/Al_2O_3, (c) Pt_2–Fe/Al_2O_3, (d) Pt–Fe/Al_2O_3 and (e) Pt–Fe_2/Al_2O_3.

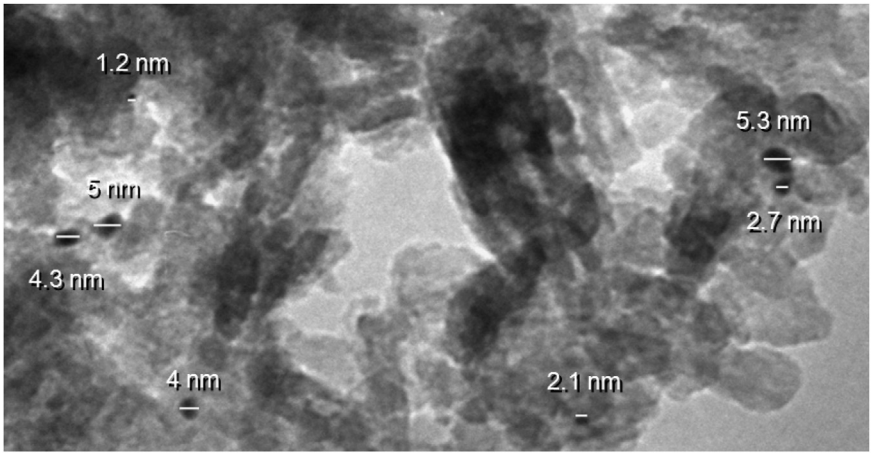

Fig. 9. Detail of the TEM images of catalyst Pt/Al_2O_3 indicating the size of Pt particles.

mercially available Al_2O_3 powder, and the pore diameter taken from BJH method was 22.3 nm for the lowest pore volume catalyst. Considering a tortuosity of 0.75, porosity of 0.8, and a ratio of $r_{molecule}/r_{pore} = 0.1$, the effective diffusion coefficient was estimated to be $D^{eff} = 1.36 \times 10^{-7}$ cm^2/s[47]. In the most limiting case for the highest reaction rate, the value of the Weisz–Prater modulus was found to be $\Psi = 0.012$, much lower than unity, and therefore

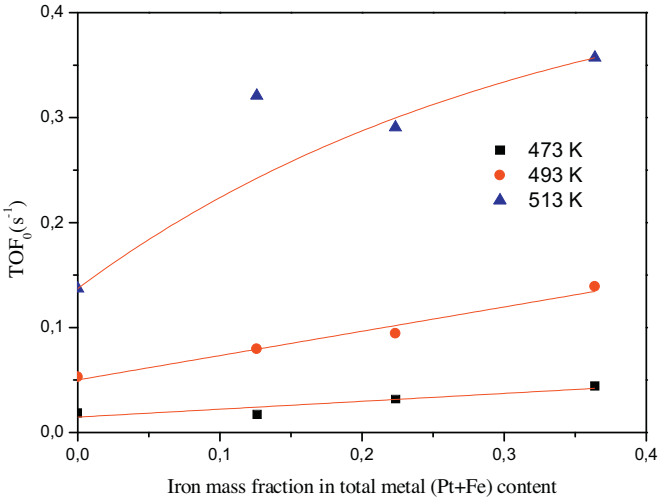

Fig. 10. Dependence of the turnover frequency of the glycerol hydrogenolysis reaction with iron content in P–Fe catalysts.

suitable for reaction rate evaluation, absent from mass transfer limitations.

The obtained results for the activity of the catalysts for glycerol hydrogenolysis are available in Table 3. Table 4 displays the reaction rates and the respective initial turnover frequencies (TOF_0) for each temperature and catalyst used. Conversion, X, was calculated according to Eq. (1), the yield of the liquid product i, Y_i, is defined in Eq. (2), and the respective selectivity, S_i, follows in Eq. (3).

$$X = \frac{\left(n_{0,\text{Glycerol}} - n_{\text{Glycerol}}\right)}{n_{0,\text{Glycerol}}} \times 100\% \quad (1)$$

$$Y_i = \frac{n_i}{n_{0,\text{Glycerol}}} \times 100\% \quad (2)$$

$$S_i = \frac{Y_i}{X} \times 100\% \quad (3)$$

For the APR reactions, since the produced hydrogen is not part of the carbon balance, the H_2 yield (Eq. (4)) was calculated as the quantity of H_2 produced over the converted glycerol.

$$H_2\text{Yield} = \frac{n_{H_2}}{n_{\text{ConvertedGlycerol}}} \times 100\%$$

The calculation of the initial turnover frequencies (TOF_0) may be of some difficulty [48]. In this work, they were estimated from initial reaction rates, and H_2 adsorption was used as a measurement of the number of active sites. As it can be seen in Fig. 10, for temperatures around 493 K, the initial turnover frequency increases almost linearly with the iron fraction in the active bimetallic particles, but higher temperatures lead to nonlinear relations between the TOF_0 and the iron content. A high selectivity towards 1,2-PD could be achieved by using milder temperatures (473 K). For higher temperatures, the production of 1-PrOH was of the same magnitude as 1,2-PD. While Fe/Al_2O_3 did not display any activity, all bimetallic Pt–Fe catalysts were more active and more selective towards 1,2-PD and 1-PrOH than Pt/Al_2O_3. This may be explained by an ensemble effect, since Fe and Pt may combine to form alloys [49].

Fig. 11 shows the glycerol concentration decay through time for all Pt-containing catalysts, to which first order apparent kinetics was used to fit the hydrogenolysis reaction. Recycle and APR results are shown in Tables 5 and 6, respectively. As demonstrated by Ravenelle et al. [50,51], the presence of hot liquid water affects γ-Al_2O_3 stability, causing it to undergo a complete phase transition to boehmite within 10 h. But Pt/Al_2O_3 catalysts prepared by impregnation of H_2PtCl_6 have an extra stability to this transition.

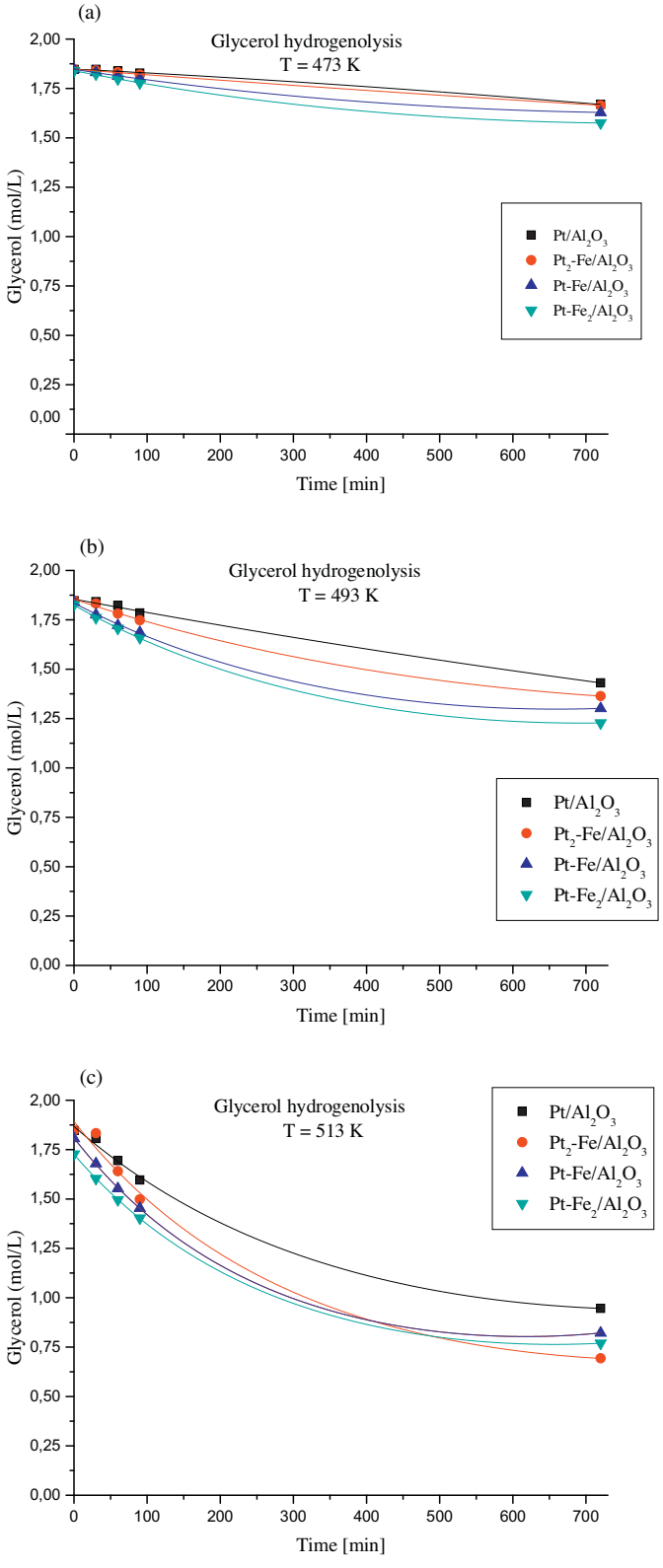

Fig. 11. Glycerol concentration decay for Pt/Al_2O_3 and Pt_x–Fe_y/Al_2O_3 catalysts at (a) 473 K, (b) 493 K and (c) 513 K.

According to the reports [50,51], the total boehmite fraction is expected to be around 0.6 for 1%wt. impregnated Pt content. In all cases, it is safe to infer that the support's activity is not the same at the beginning and at the end of the reaction. However, the recycle experiments done in this work show that the boehmite formation

Table 3
Conversion and product selectivity for glycerol hydrogenolysis over Pt–Fe/Al_2O_3 catalysts.

Catalyst	Temperature (K)	Conversion (%)	Selectivity (%)					
			1,2-PD	EG	1,3-PD	1-PrOH	Ethanol	Others[a]
Pt/Al_2O_3	473	9.6	66.0	13.0	3.7	7.9	8.0	1.4
Pt/Al_2O_3	493	22.5	49.4	10.7	4.0	23.5	10.8	1.6
Pt/Al_2O_3	513	48.8	50.5	6.7	1.4	31.5	6.9	3.0
Fe/Al_2O_3	513	<1	–	–	-	–	–	–
Pt_2–Fe/Al_2O_3	473	9.9	76.0	9.1	2.0	4.6	7.1	1.2
Pt_2–Fe/Al_2O_3	493	26.2	67.3	9.1	1.7	12.8	8.2	1.0
Pt_2–Fe/Al_2O_3	513	62.4	35.5	5.3	0.8	43.7	7.7	6.9
Pt–Fe/Al_2O_3	473	11.8	71.8	9.3	2.5	7.6	6.6	2.1
Pt–Fe/Al_2O_3	493	29.5	55.8	8.0	2.1	23.0	8.0	3.0
Pt–Fe/Al_2O_3	513	55.5	33.7	5.7	1.5	43.6	9.0	6.6
Pt–Fe_2/Al_2O_3	473	14.7	77.1	9.8	1.9	6.1	3.8	1.3
Pt–Fe_2/Al_2O_3	493	33.5	62.7	8.8	1.3	18.0	5.5	3.6
Pt–Fe_2/Al_2O_3	513	58.3	37.9	6.0	1.0	39.7	7.5	7.8

Conditions: 26.2 bar abs. initial H_2, 0.5 g catalyst, 500 rpm, 150 mL of 20%wt. glycerol solution, and 12 h batch.
[a] Others: methanol, acetone, acetol, propanal, acetic acid, propanoic acid, carbon dioxide.

Table 4
Reaction rate constants of first order apparent kinetic fit, and turnover frequencies for Pt_x–Fe_y/Al_2O_3 catalysts in glycerol hydrogenolysis.

Catalyst	Temp. (K)	k_{app} (10^{-3} L.g_{cat}^{-1} h^{-1})	TOF_0 ($10^{-2}s^{-1}$)	r^{2a}
Pt/Al_2O_3	473	2.4	1.9	1.000
Pt/Al_2O_3	493	6.0	5.3	0.998
Pt/Al_2O_3	513	14.6	13.7	0.989
Pt_2–Fe/Al_2O_3	473	2.4	1.7	0.999
Pt_2–Fe/Al_2O_3	493	6.8	8.0	0.994
Pt_2–Fe/Al_2O_3	513	21.8	32.1	0.985
Pt–Fe/Al_2O_3	473	2.9	3.2	0.992
Pt–Fe/Al_2O_3	493	7.7	9.4	0.981
Pt–Fe/Al_2O_3	513	17.5	29.1	0.975
Pt–Fe_2/Al_2O_3	473	3.6	4.4	0.990
Pt–Fe_2/Al_2O_3	493	9.0	13.9	0.985
Pt–Fe_2/Al_2O_3	513	18.1	35.7	0.981

[a] r: Correlation coefficient from least squares.

Table 5
Recycle results for monometallic Pt/Al_2O_3 and bimetallic Pt_x–Fe_y/Al_2O_3 catalysts for glycerol hydrogenolysis.

Catalyst	Original batch conversion (%)	Recycle conversion (%)	Selectivity of recycling experiments (%)				
			1,2-PD	EG	1-PrOH	Ethanol	Others[a]
Pt/Al_2O_3	22.5	22.0	58.5	9.6	14.5	12.3	5.1
Pt_2–Fe/Al_2O_3	26.2	26.1	61.1	9.5	14.6	9.6	5.2
Pt–Fe/Al_2O_3	29.5	26.1	61.1	9.5	14.6	9.6	5.2
Pt–Fe_2/Al_2O_3	33.5	25.9	61.2	10.0	15.3	8.2	5.3

Conditions: 26.2 bar abs initial H_2, 0.5 g catalyst, 500 rpm, 150 mL of 20%wt. glycerol solution, 12 h batch, and 493 K.
[a] Others: 1,3-PD, methanol, acetol, acetone, propanal, acetic acid, propanoic acid, carbon dioxide, etc.

Table 6
APR results for monometallic Pt/Al_2O_3 and bimetallic Pt_x–Fe_y/Al_2O_3 catalysts.

Catalyst	Conversion (%)	Selectivity/yield (%)						
		1,2-PD	EG	1-PrOH	Ethanol	Acetol	Others[a]	H_2
Pt/Al_2O_3	42.9	22.4	2.6	50.2	17.7	4.1	3.0	10.0
Pt_2–Fe/Al_2O_3	61.2	23.3	2.8	46.9	16.2	5.4	5.4	12.5
Pt–Fe/Al_2O_3	60.5	26.9	3.7	39.4	12.6	8.2	9.2	11.5
Pt–Fe_2/Al_2O_3	62.1	25.6	3.8	38.9	11.2	8.9	11.7	9.8

Conditions: 11.4 bar abs initial N_2, 0.5 g catalyst, 500 rpm, 150 mL of 20%wt. glycerol solution, 12 h batch, and 513 K.
[a] Others: liquid phase products and dissolved gas such as CO_2, 1,3-PD, methanol, acetone, propanal, acetic acid,propanoic acid, etc.

can be one cause for the activity drop, but not the most relevant, since the expected extent of the phase transition from Al_2O_3 to AlO(OH) would have a much more pronounced effect in lowering the conversion, than the observed activity decrease. The increment in Fe content shows a significant negative effect on catalyst stability, which seems to have a greater impact than the support's phase transition.

From the results of APR reactions, the monometallic Pt catalyst showed the best selectivity towards 1-PrOH, higher than the one presented in glycerol hydrogenolysis. Huber et al. [33]. have conducted APR experiments using ethylene glycol with high throughput reactors over Pt–Fe/Al_2O_3 catalysts. Their results are in agreement with the present work regarding the promotional effect of Fe for H_2 production, which is limited. The main reason for undertaking glycerol APR reactions was to test whether the

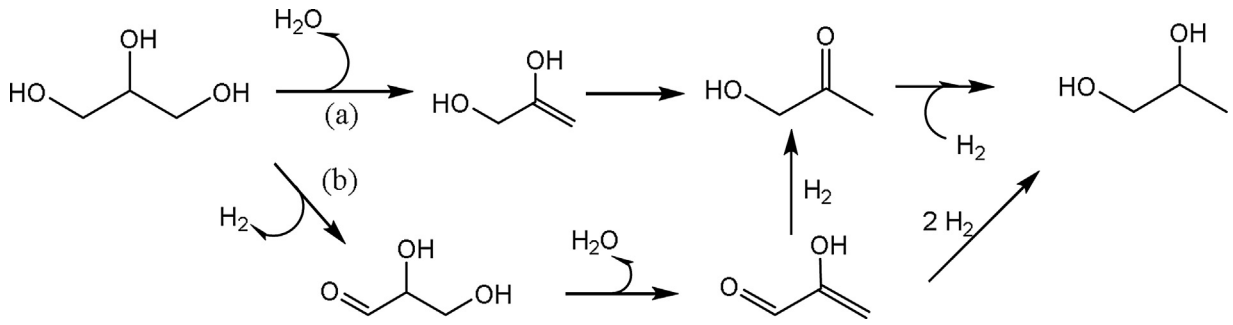

Fig. 12. Scheme of glycerol hydrogenolysis having acetol as an intermediate, based on Refs. [53–56].

adsorbed hydrogen on the catalytic sites responsible for glycerol hydrogenolysis was only provided by the externally fed H_2 or generated *in situ*, as part of the glycerol dehydrogenation mechanism and/or other reactions, such as water-gas shift reaction (WGSR). As it happens, the detection of sizeable H_2 quantities in the gas phase produced by APR reaction indicates that 1,2-PD and 1-PrOH are also produced at temperatures above 493 K without the use of external hydrogen There was a considerable drop in selectivity towards the production of 1,3-PD (almost none), an increase in ethanol, and a remarkable presence of acetol in the APR process. The 1-PrOH selectivity is clearly inversely proportional to the iron content in the catalyst for APR, from which one would assume that the reaction is sensitive to the catalyst's structure. In Table 6, the values of H_2 yield are shown, according to eq. 4, and these results are in agreement with other APR works [26–34]. It should also be noted that through bimetallic catalysts, hydrogen production is slightly lessened with increasing Fe content. Therefore, optimal Fe fractions in the catalyst for H_2 production seem to be low.

The behavior of the hydrogenolysis reaction is very different from APR. While in the hydrogenolysis there is consumption of the externally fed H_2, and consequently a pressure drop throughout the batch, in APR there is a remarkable increase in the pressure. In all APR experiments the final pressure was about 21.8 bar at environment temperature, contrasting with the initial 11.3 bar of inert N_2. In the gas phase there was CO_2, H_2, methane, ethane and traces of other products.

In view of the obtained catalytic results and material characterizations, a model for the surface activity may be advanced. For the present range of Fe composition, the TOF_0 values clearly indicate catalyst activity increase with increasing iron content. Considering the TPR profiles, the combination of Pt and Fe causes an enhancement in the amount of Fe atoms that can be reduced at lower temperatures. For the reduction temperature used (723 K), all platinum containing catalysts are expected to act in the form of totally reduced nanoparticles. Therefore, the extra catalytic activity observed for the Pt_x–Fe_y catalysts appears to be due to reduced Fe atoms on the bimetallic particles. From the FT-IR spectra of the bimetallic catalysts, there is no intensity decrease at 2060 cm^{-1}, the characteristic frequency for CO adsorption onto Pt sites, and there is a relevant different band around 2040 cm^{-1}, suggesting the presence of actual new adsorption sites from the Pt–Fe interaction, assigned to CO linear adsorption at reduced Fe sites [35,39]. The adsorption band remains broad up to 573 K (Fig. 4), making it plausible that reduced Fe atoms are actually active in the reaction. Both metallic Pt and Fe present cubic structures: Pt has an fcc structure (Fm-3m), while Fe has a bcc one (Im-3m). Therefore, the bimetallic particles are expected to have a cubic structure, in which the minority element is immersed in a phase of the majority element, and is diluted on the surface. However, given its much lower melting point and atomic weight, Fe should be more mobile, and therefore constitute external layers of the bimetallic particle, which is corroborated both by lower H/Pt ratios with increasing Fe from chemisorption analysis, and XPS analysis from calcined and passivated Pt_2–Fe catalyst, to which Pt dilution occurs in the bimetallic particle formation process.

It has been demonstrated that overlayers of one metal onto another cause a shift in the d band energy of the whole particle [52]. Accordingly, when an overlayer of Fe atoms forms onto a Pt particle, the d band energy is shifted to higher values, which translates into an increase in catalyst activity. The overall d band energy of the bimetallic particle is higher than for a monometallic Pt particle, but the d band occupancy of the Fe atoms is low in comparison with Pt atoms, which should have an increase in electron density of Pt atoms in Pt–Fe nanoparticles [35]. This makes adsorption phenomena likely to be optimal at the Fe available sites (not too strong, not too weak), and electron donation likely to occur on Pt atoms. An increase in activity by formation of new Pt–Fe interactions is precisely what is observed in the present work, and therefore overlayers of Fe atoms onto Pt particles seem to be a reasonable explanation for the extra activity of the Pt–Fe catalysts.

Three main mechanisms are well accepted for glycerol hydrogenolysis, namely, (a) the dehydrogenation-dehydration-hydrogenation route, (b) the dehydration-hydrogenation route and (c) the direct hydrogenolysis route [53]. They differ essentially on the acidity of the catalytic sites for the first step, and except for route (c), which is related to 1,3-PD and 1,2-PD via carbenium ions as intermediates, the other routes involve the formation of an unstable enol at some point. Fig. 12 summarizes routes of 1,2-PD formation portraying acetol as an intermediate. Over acid sites [54], acetol in route (a) is believed to be generated after glycerol dehydration and enol-keto tautomerization. In route (b), glycerol is dehydrogenated into glyceraldehyde, which is dehydrated to hydroxyl-acrolein, which later can form acetol [55,56]. For both mechanisms, a final carbonyl hydrogenation of acetol occurs on the active metal, forming 1,2-PD. Since no acetol is produced by glycerol dehydration over pure Al_2O_3 [57] or other supports [56,58], it is argued that the active metal phase plays an important role not only in the hydrogenation, but also in the first steps of the reaction. In view of this, as it can be seen in Fig. 10, contrary to what would be commonly expected [36], the reaction rate is increased by the increment in iron content, regardless of the decrease in the capacity to chemisorb hydrogen. This means that the bimetallic Pt–Fe particles do not adsorb H_2 as well as monometallic Pt, but in comparison they do adsorb glycerol better. It also means that the steps prior to acetol hydrogenation should be the limiting ones. In other words, the extra activity of the bimetallic catalysts should rely on an incremented ability to adsorb and dehydrate or dehydrogenate glycerol, rather than only catalyzing the hydrogenation of the carbonyl group. This can be attributed to the effect of the positive d band shift caused by overlayers of Fe atoms onto Pt atoms [52]. Within the studied Fe content range,

the active Pt–Fe phase shows increasing activity with increasing Fe content, seemingly because of its ability to dehydrate and dehydrogenate glycerol. There is a possibility that the iron content is still too low to impact considerably the hydrogen adsorption, and is yet to be increased in order to negatively affect the reaction rate. In any case, the ensemble effect obtained from Pt–Fe and the reduced Fe overlayers are desirable for glycerol conversion.

4. Conclusions

Glycerol hydrogenolysis and APR are important reactions in biomass valorization, rendering inevitable industrial interests, to which Pt-based catalysts show promise, especially since common hydrocarbon reforming operation using platinum-based catalysts are typically undertaken at 773 K, for non-renewables [59,60]. The bimetallic Pt_x–Fe_y/Al_2O_3 catalysts presented in this work seem to be viable materials towards accomplishing both reactions, displaying better performance in activity and in selectivity towards 1,2-PD and 1-PrOH than monometallic Pt/Al_2O_3 for glycerol hydrogenolysis, whereas in the APR reaction the situation is inverse. Metallic interaction between Pt and Fe is evident, and reduced Fe overlayers onto Pt particles are considered the cause for better bimetallic activity. Through APR reaction tests it is clear that hydrogen is generated at the catalytic sites as part of glycerol conversion. The advantage of using Fe as a promoter for Pt, instead of another metal, is enormous, given the cost and abundance of Fe.

Acknowledgements

The authors would like to thank CNPq, FAPERJ and CAPES for financial support.

References

[1] G. Knothe, J. Van Gerpen, J. Krahl, The Biodiesel Handbook, AOCS Press, Champaign, Illinois, 2005.
[2] C.A.G. Quispe, C.J.R. Coronado, J.A. Carvalho Jr., Renew. Sustain. Energy Rev. 27 (2013) 475–493.
[3] C.J.A. Mota, C.X.A. da Silva, V.L.C. Goncalves, Quim. Nova 32 (2009) 639–648.
[4] J.N. Beltramini, C. Zhou, Thermochemical Conversion of Biomass to Liquid Fuels and Chemicals, in: M. Crocker (Ed.), RSC Publishing, Cambridge, 2010, pp. 435–467.
[5] BRAZIL; Casa Civil, Federal Law Nr. 13.033, 2014. Available at http://www.planalto.gov.br/ccivil_03/_Ato2011-2014/2014/Lei/L13033.htm.
[6] BRAZIL, Agência Nacional de Petróleo, Gás Natural e Biocombustíveis (ANP). Boletim Mensal do Biodiesel–Ferbuary 2015. Available at www.anp.gov.br.
[7] Y. Nakagawa, K. Tomishige, Catal. Sci. Technol. 1 (2011) 179–190.
[8] Y. Nakagawa, Y. Shinmi, S. Koso, K. Tomishige, J. Catal. 272 (2010) 191–194.
[9] H. Liu, S. Liang, T. Jiang, B. Han, Y. Zhou, Clean–Soil Air Water 40 (2010) 318–324.
[10] E. Kravela, R. Palcheva, L. Dimitrov, U. Armbruster, A. Brückner, A. Spojakina, J. Mater. Sci. 46 (2011) 7160–7168.
[11] Y. Liu, H. Tüysüz, C.J. Jia, M. Schwickardi, R. Rinaldi, A.H. Lu, W. Schmidt, F. Schüth, Chem. Commun. 46 (2010) 1238–1240.
[12] M.A. Dasari, P.P. Kiatsimkul, W.R. Sutterlin, G.J. Suppes, Appl. Catal. A 281 (2005) 225–231.
[13] Z. Yuan, P. Wu, J. Gao, X. Lu, Z. Hou, X. Zheng, Catal. Lett. 130 (2009) 261–265.
[14] A. Wawrzetz, B. Peng, A. Hrabar, A. Jentys, A.A. Lemonidou, J.A. Lercher, J. Catal. 269 (2010) 411–420.
[15] I. Gandarias, P.L. Arias, J. Requies, M.B. Güemez, J.L.G. Fierro, Appl. Catal. B 97 (2010) 248–256.
[16] N. Ueda, Y. Nakagawa, K. Tomishige, Chem. Lett. 139 (2010) 506–507.
[17] T. Kurosaka, H. Maruyama, I. Naribayashi, Y. Sasaki, Catal. Commun. 9 (2008) 1360–1363.
[18] O.M. Daniel, A. De La Riva, E.L. Kunkes, A.K. Datye, J.A. Dumesic, R.J. Davis, ChemCatChem 2 (2010) 1107–1114.
[19] A. Brandner, K. Lehnert, A. Bienholz, M. Lucas, P. Claus, Top. Catal. 52 (2009) 278–287.
[20] D. Roy, B. Subramaniam, R.V. Chaudhari, Catal. Today 156 (2010) 31–37.
[21] L. Gong, Y. Lu, Y. Ding, R. Lin, J. Li, W. Dong, T. Wang, W. Chen, Appl. Catal. A 390 (2010) 119–126.
[22] J. Oh, S. Dash, H. Lee, Green Chem. 13 (2011) 2004–2007.
[23] J. ten Dam, F. Kapteijn, K. Djianashvili, U. Hanefeld, Catal. Commun. 13 (2011) 1–5.
[24] J. ten Dam, F. Kapteijn, K. Djianashvili, U. Hanefeld, ChemCatChem. 5 (2013) 497–505.
[25] M. Checa, F. Auneau, J. Hidalgo-Carrillo, A. Marinas, J.M. Marinas, C. Pinel, F.J. Urbano, Catal.Today 196 (2012) 91–100.
[26] M.L. Barbelli, F. Pompeo, G.F. Santori, N.N. Nichio, Catal. Today 213 (2013) 58–64.
[27] V.V. Ordomsky, A.Y. Khodakov, Green Chem. 16 (2014) 2128–2131.
[28] A. Ciftci, S. Eren, D.A.J.M. Lighthart, E.J.M. Hensen, ChemCatChem. 6 (2014) 1260–1269.
[29] M.M. Rahman, T.L. Church, M.F. Variava, A.T. Harris, A.I. Minett, RSC Adv. 4 (2014) 18951–18960.
[30] A. Ciftci, D.A.J.M. Lighthart, E.J.M. Hensen, Green Chem. 16 (2014) 853–863.
[31] M. El Doukkali, A. Iriondo, J.F. Cambra, I. Gandarias, L. Jalowiecki-Duhamel, F. Dumeignil, P.L. Arias, Appl. Catal. A 472 (2014) 80–91.
[32] E.S. Vasiliadou, A.A. Lemonidou, Catalysts 4 (2014) 397–413.
[33] G.W. Huber, J.W. Shabaker, S.T. Evans, J.A. Dumesic, Appl. Catal. B Environ. 62 (2006) 226–235.
[34] J. Lee, Y.T. Kim, G.W. Huber, Green Chem. 16 (2014) 708–718.
[35] A. Siani, O.S. Alexeev, G. Lafaye, M.D. Amiridis, J. Catal. 266 (2009) 26–38.
[36] J. Sinfelt, Acc. Chem. Res. 10 (1977) 134–139.
[37] L. Guczi, K. Matusek, M. Eszterle, J. Catal. 60 (1979) 121–132.
[38] K.S.W. Sing, Pure Appl. Chem. 54 (1982), 2201–2218.
[39] C. Johnston, N. Jorgensen, C.H. Rochester, J. Chem. Soc. Faraday Trans. I 84 (1988) 3605–3613.
[40] F.B. Passos, M. Schmal, M.A. Vannice, J. Catal. 160 (1996) 106–117.
[41] E.V. Benvenutti, L. Franken, C.C. Moro, C.U. Davanzo, Langmuir 15 (1999) 8140–8146.
[42] J.Z. Shyu, K. Otto, J. Catal. 115 (1989) 16–23.
[43] J.Z. Shyu, K. Otto, Appl. Surf. Sci. 32 (1988) 246–252.
[44] J.F. Moulder, W.F. Stickle, P.E. Sobol, K.D. Bomben, Handbook of Photoelectron Spectroscopy, Physical Electronics Division, 1992.
[45] B.J. Kip, F.B.M. Duivenvoorden, D.C. Koningsberger, R. Prins, J. Am. Chem. Soc. 108 (1986) 5633–5634.
[46] M.A. Vannice, Kinetics of Catalytic Reactions, Springer, 2005.
[47] Physical Properties of Glycerine and its solutions, Hydrocarbon Process. 1967.
[48] M. Boudart, Chem. Rev. 95 (1995) 661–666.
[49] A. Christensen, A.V. Ruban, P. Stoltze, P.W. Jacobsen, H.L. Skriver, J.K. Nørskov, F. Besenbacher, Phys. Rev. B 56 (1997) 5822–5834.
[50] R.M. Ravenelle, J.R. Copeland, W.-G. Kim, J.C. Crittenden, C. Sievers, ACS Catal. 1 (2011) 552–561.
[51] R.M. Ravenelle, F.Z. Diallo, J.C. Crittenden, C. Sievers, Chemcatchem 4 (2012) 492–494.
[52] A. Ruban, B. Hammer, P. Stoltze, H.L. Skriver, J.K. Norskov, J. Mol. Catal. A-Chem. 115 (1997) 421–429.
[53] A. Martin, U. Armbruster, I. Gandarias, P.L. Arias, Eur. J. Lipid Sci. Technol. 115 (2013) 9–27.
[54] M. Balaraju, K. Jagadeeswaraiah, P.S. Sai Prasad, N. Lingaiah, Catal. Sci. Technol. 2 (2012) 1967–1976.
[55] C. Montassier, J.C. Ménézo, L.C. Hoang, C. Renaud, J. Barbier, J. Mol. Catal. 70 (1991) 99–110.
[56] A. Alhanash, E.F. Kozhevnikova, I.V. Kozhevnikov, Catal. Lett. 120 (2008) 307–311.
[57] X. Lin, Y. Lv, Y. Xi, Y. Qu, D.L. Phillips, C. Liu, Energy Fuels 28 (2014) 3345–3351.
[58] J.B. Salazar, D.D. Falcone, H.N. Pham, A.K. Datye, F.B. Passos, R.J. Davis, Appl. Catal. A-Gen. 482 (2014) 137–144.
[59] M.R. Rahimpour, M. Jafari, D. Iranshahi, Appl. Energy 109 (2013) 79–93.
[60] J.J.H.B. Sattler, J. Ruiz-Martinez, E. Santillan-Jimenez, B.M. Weckhuysen, Chem. Rev. 114 (2014) 10613–10653.